



OPEN

## Osteogenesis in human periodontal ligament stem cell sheets is enhanced by the protease-activated receptor 1 (PAR<sub>1</sub>) in vivo

Tomaz Alves<sup>1,2</sup>, Leticia M. Gasparoni<sup>2</sup>, Danilo Balzarini<sup>2</sup>, Emmanuel Albuquerque-Souza<sup>2,3</sup>, Vichor de Oliveira<sup>4</sup>, Emanuel S. Rovai<sup>5</sup>, Jose da Silva<sup>2</sup>, Aldrin Huamán-Mendoza<sup>2</sup>, Luiz H. Catalani<sup>6</sup>, Carla R. Sipert<sup>7</sup> & Marinella Holzhausen<sup>2</sup>✉

Human periodontal ligament stem cells (PDLSCs) have been studied as a promising strategy in regenerative approaches. The protease-activated receptor 1 (PAR<sub>1</sub>) plays a key role in osteogenesis and has been shown to induce osteogenesis and increase bone formation in PDLSCs. However, little is known about its effects when activated in PDLSCs as a cell sheet construct and how it would impact bone formation as a graft in vivo. Here, PDLSCs were obtained from 3 patients. Groups were divided into control, osteogenic medium and osteogenic medium + PAR<sub>1</sub> activation by TFLLR-NH2 peptide. Cell phenotype was determined by flow cytometry and immunofluorescence. Calcium deposition was quantified by Alizarin Red Staining. Cell sheet microstructure was analyzed through light, scanning electron microscopy and histology and transplanted to Balb/c nude mice. Immunohistochemistry for bone sialoprotein (BSP), integrin β1 and collagen type 1 and histological stains (H&E, Van Giesson, Masson's Trichrome and Von Kossa) were performed on the ex-vivo mineralized tissue after 60 days of implantation in vivo. Ectopic bone formation was evaluated through micro-CT. PAR<sub>1</sub> activation increased calcium deposition in vitro as well as BSP, collagen type 1 and integrin β1 protein expression and higher ectopic bone formation (micro-CT) in vivo.

Periodontal disease is a chronic inflammatory condition characterized by a dysbiotic microbiome mediated by host response patterns, which in advanced stages may result in a substantial breakdown of the tooth-supporting tissues, ultimately leading to tooth loss<sup>1</sup>. Periodontal tissue is a specialized distinctive structure composed by the alveolar bone, cementum and periodontal ligament. Damage to these structures severely compromises important biological functions, including bone remodeling, occlusal forces absorption and the masticatory function<sup>1</sup>.

Current both non-surgical and surgical treatments such as guided tissue regeneration (GTR) and guided bone regeneration (GBR) have been widely utilized in the clinical practice with the aim to eliminate the infection's primary cause and achieve regeneration, respectively. However, these treatment strategies have been shown to be ineffective in providing complete regeneration of hard and soft periodontal structures and the most common outcome is the formation of long junctional epithelium or the incomplete regeneration of the periodontal structures, and a long-term stable clinical regenerative outcome has not been yet achieved<sup>2-4</sup>.

Recently, several studies in the cell-based regenerative medicine field have been reported combining tissue engineering and stem cells<sup>5-7</sup>. The use of cell sheets is a promising therapeutic strategy that allows the use of

<sup>1</sup>Division of Comprehensive Oral Health, Adams School of Dentistry, University of North Carolina, Chapel Hill, NC, USA. <sup>2</sup>Division of Periodontology, Department of Stomatology, School of Dentistry, University of São Paulo, São Paulo, SP 05508-000, Brazil. <sup>3</sup>Department of Periodontics, School of Dental Medicine, University of Pennsylvania, Philadelphia, PA, USA. <sup>4</sup>Division of Anatomy, Institute of Biomedical Sciences, University of São Paulo, São Paulo, SP 05508-000, Brazil. <sup>5</sup>Division of Periodontology, Dental School, University of Taubate, Taubaté, SP 12020-340, Brazil. <sup>6</sup>Department of Fundamental Chemistry, Institute of Chemistry, University of São Paulo, São Paulo, SP 05508-900, Brazil. <sup>7</sup>Division of Endodontics, Department of Dentistry, School of Dentistry, University of São Paulo, São Paulo, SP 05508-000, Brazil. ✉email: marinella@usp.br

mesenchymal stem cells in a construct that maintains interconnected cells in contact with their extracellular matrix, providing stability and allowing delivery to possible therapies<sup>8</sup>. Cell sheets utilizing PDLSCs are well known to mimize the natural periodontal ligament environment in a regenerative state and to enhance cellular signal communications that potentially stimulate regeneration of periodontal tissues<sup>3</sup>.

The protease-activated receptor type 1 (PAR<sub>1</sub>) is a G protein-coupled cell membrane receptor that regulates several intracellular signaling pathways related to enhancement of osteogenic differentiation, increase in mineralized matrix deposition and upregulation of cementogenic gene expression as well<sup>9</sup>. PAR<sub>1</sub> activation plays a key role in osteogenesis and bone regeneration<sup>5,10</sup> by enhancing osteoblast proliferation and differentiation<sup>11</sup>, increasing the synthesis of osteoprotegerin (OPG) in periodontal ligament cells and reducing the inflammatory osteoclastogenesis induced by LPS<sup>12</sup>. Furthermore, PAR<sub>1</sub> has been shown to be associated with vascular and coagulatory processes<sup>13</sup> as well as bone formation and osteoclasts differentiation impairment at bone healing early stages in an animal model<sup>14</sup>.

Whether PAR<sub>1</sub> shows an effect on PDLSCs in a cell sheet in vivo model is still unknown. This present study focused on investigating PAR<sub>1</sub> activation on the PDLSCs cell sheet outcome in an in vivo model.

## Results

**Periodontal ligament isolated cells present a diverse phenotypic population.** We isolated PDLSCs from third molars from 3 individuals (I1, I2 and I3) and characterized the cell lines by flow cytometry and immunofluorescence for PAR<sub>1</sub> (Fig. 1A). Although all cell lines were positive for pluripotency surface markers (Fig. 1C), only I2 presented a positive phenotypic profile for OCT-4 (22%), SOX2 (13.2%), and STRO-1 (72.6%) in agreement with the literature to be considered a PDLSC lineage (Fig. 1B and Supp. 1 A,B)<sup>15</sup>. Further, I2 presented a high percentage of PAR<sub>1</sub> positive PDLSCs (~100%), as observed by Flow Cytometry and Immunofluorescence (Fig. 1B,C).

The Alizarin Red staining was carried out using only the I2 isolated mesenchymal stem cell line to evaluate whether the PAR<sub>1</sub> activation played a role in their osteogenic differentiation and calcium deposition. Here, PAR<sub>1</sub> significantly promoted an increase in calcium deposits through ARS assay in I2 PDLSCs (Fig. 1D). This way, we proceeded to perform further experiments using only the I2 cell line.

**Cell sheets characterization.** We characterized PDLSC sheets by scanning electron microscopy (SEM), H&E and direct light microscopy (Fig. 2A). After 14 days of culture with the three different groups, PDLSC sheets were fully formed and ready to undergo full detachment from the dishes (Supp. 2B). Light microscopy images showed a confluent fibroblastic-like profile as expected (Fig. 2B). Furthermore, qualitative analysis of the H&E sections detected differences in cell sheet thickness degree in the OST and OST + PAR<sub>1</sub> groups when compared with the CTRL group (Fig. 2B).

**PAR<sub>1</sub> activation in PDLSCs cell sheets enhanced mineralization after in vivo transplantation.** In order to evaluate the osteogenic potential of PAR<sub>1</sub> activation in PDLSCs sheets, we performed in vivo experiments by transplanting cell sheets into the subcutaneous of Balb/c nude mice to evaluate the ectopic bone formation through micro-CT after a 60-days period (Fig. 3A). Micro-CT results were displayed in bone volume/tissue volume percentage (BV/TV %) (Fig. 3B). The OST + PAR<sub>1</sub> group demonstrated a higher ectopic bone formation outcome in comparison with the other groups ( $p < 0.05$ ) (Fig. 3B).

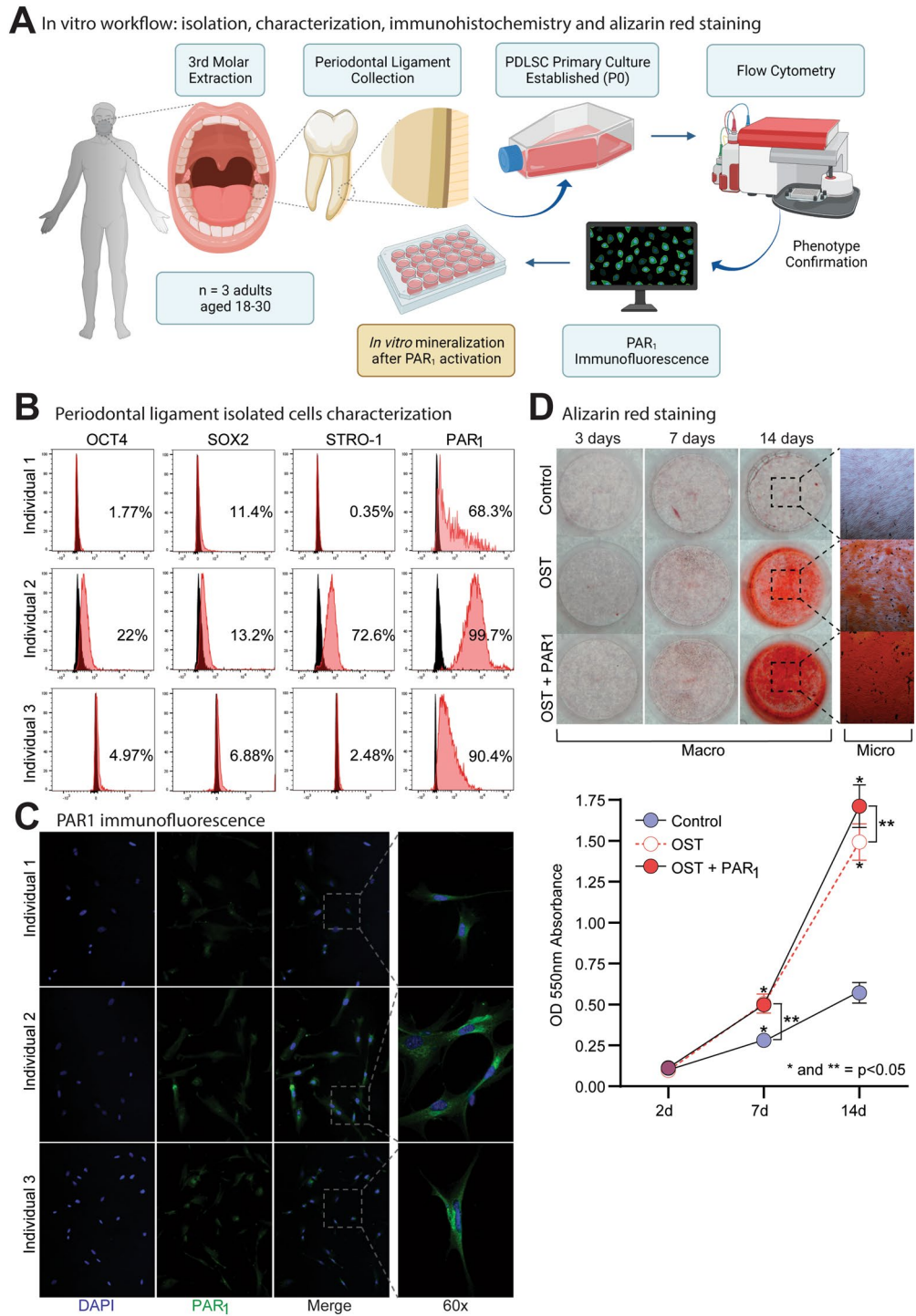
**PAR<sub>1</sub> activation mediates osteogenesis in PDLSC sheets in vivo.** Histological qualitative analysis from H&E, Masson Trichrome, Van Gieson and Von Kossa stains from the 3 groups after a 2-month transplantation period in Balb/c nude mice suggested an increased osteogenic process displayed by greater presence of osteoblast clusters and lower abundance of undifferentiated fibroblast-like cells for the OST + PAR<sub>1</sub> group (Fig. 4A) and increased calcium deposition in the neoformed bone matrix (Fig. 4B) when compared to the OST and CTRL groups (Fig. 4A,B). Furthermore, a qualitative analysis suggested a higher number of vessels in the OST group when compared to the other groups, suggesting that this group was in an intermediate osteogenesis stage when compared to the OST + PAR<sub>1</sub> group (Fig. 4A).

**PAR<sub>1</sub>-induced mineralization in vivo is followed by an upregulation of osteogenic markers.** Immunohistochemistry results presented a higher positive expression of BSP in the OST + PAR<sub>1</sub> group when compared with the other groups (Fig. 5A,B). Moreover, the expression of integrin 1 $\beta$  and collagen type 1 was detected in higher levels at the OST + PAR<sub>1</sub> group when compared with the other groups (Fig. 5A,B).

## Discussion

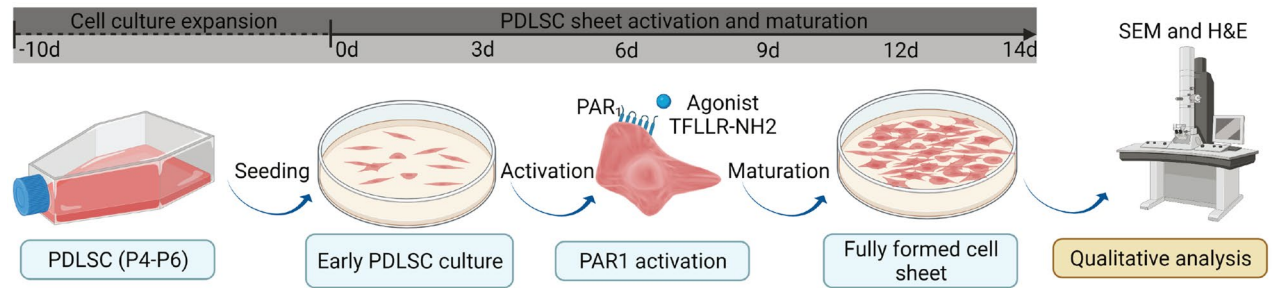
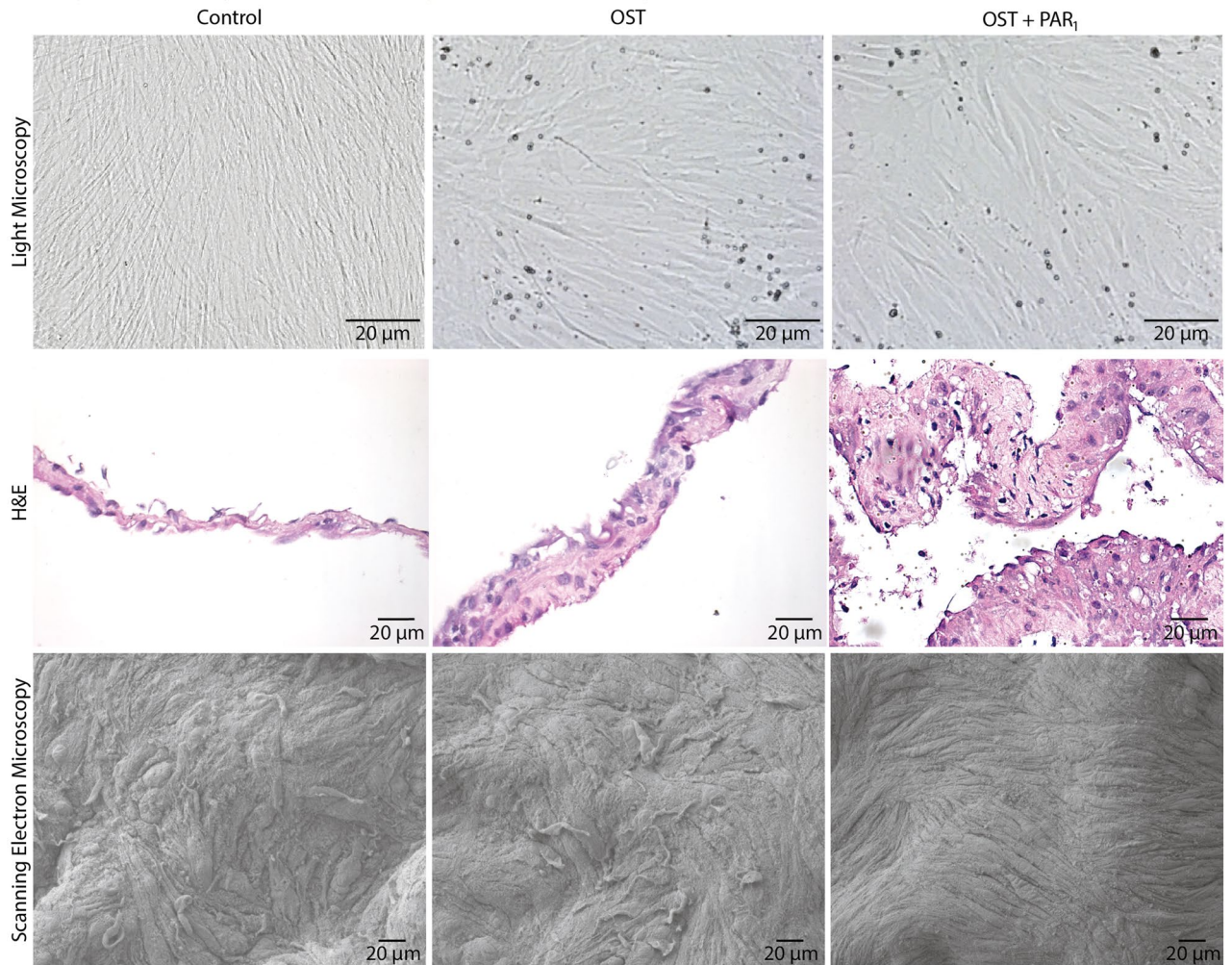
In this study, we investigated the osteogenic potential of the PAR<sub>1</sub> activation by using a cell sheet engineering strategy in an in vivo model. Previous studies have reported the role of PAR<sub>1</sub> in the osteogenic processes demonstrating that its absence is associated with derived bone marrow cells migration impairment, an increase in osteoclast colonization, enhanced osteoclastogenesis and a decrease in mineralized bone deposition in vivo<sup>14,16</sup>.

On the other hand, PAR<sub>1</sub> activation has been largely reported to upregulate bone formation by mediating proliferative responses in osteoblasts<sup>5,10,14</sup>. Our group has previously demonstrated that PAR<sub>1</sub> activation in PDLSCs is specifically associated with an increase in mineralized nodule deposition, higher calcium concentration levels and increased PDLSC proliferation. In addition, PAR<sub>1</sub> blockage decreased the calcium deposition, suggesting that PAR<sub>1</sub> plays a major role in mineralization and differentiation of PDLSCs<sup>17</sup>.



**Figure 1.** (A) Immunofluorescence, flow cytometry and alizarin red staining experiment flow. (B) Flow cytometry analysis showing the phenotypic characterization of PDLSCs for surface stemness, multipotent embryonic biomarkers (SOX2, OCT4, STRO-1) and PAR<sub>1</sub> from three individuals (I1, I2 and I3). Unstained cells were used to set positive cell populations,  $p < 0.05$ . (C) PAR<sub>1</sub> immunofluorescence expression in PDLSCs isolated cell lines. Images in 60X magnification. (D) Alizarin red staining for PDLSCs sheets (I2) after 14 days. Results are given as the mean  $\pm$  SD. Figure (A) was created using BioRender.

In the present study, we isolated PDLSCs from three patients, characterized the surface marker phenotypes by flow cytometry and purposefully proceeded to evaluate the osteogenic differentiation potential in the cell line that presented a mesenchymal profile (I2). The non-specialized mesenchymal stem cells found in the periodontal

**A** Cell sheet manufacturing and microstructure qualitative analysis workflow: light microscopy, SEM and H&E**B** Light microscopy, H&E and scanning electron microscopy

**Figure 2.** (A) Cell sheets manufacturing and macroscopic morphological characterization workflow. (B) Light microscopy (40x), cell sheet histological profile by H&E staining and microstructural analysis through scanning electron microscopy (400x) from cell sheets for the 3 experimental groups.

ligament tissue, such as PDLSCs present pluripotency properties that allow differentiation into several cell types, including osteoblasts and cementoblasts. These cells exhibit a phenotype that is compatible with the positive expression of OCT4, STRO-1, CD-44 and CD-146 cell markers<sup>18–22</sup>. Further, cells with positive expression of STRO-1 were found to be related to periodontal tissue formation and expressed in dental follicle cells in mice<sup>23,24</sup>.

Our results demonstrated a possible correlation between the presence of stemness markers (OCT4, CD146, SOX2, CD-90, STRO-1, CD-44) and PAR<sub>1</sub> prevalence, with a higher calcium deposition being found in I2 in the ARS assay, although further analysis is needed to confirm this association. At the same time, I2 was negative for CD14, CD31, and CD34, corroborating with PDLSCs phenotype present in the literature<sup>15</sup>.

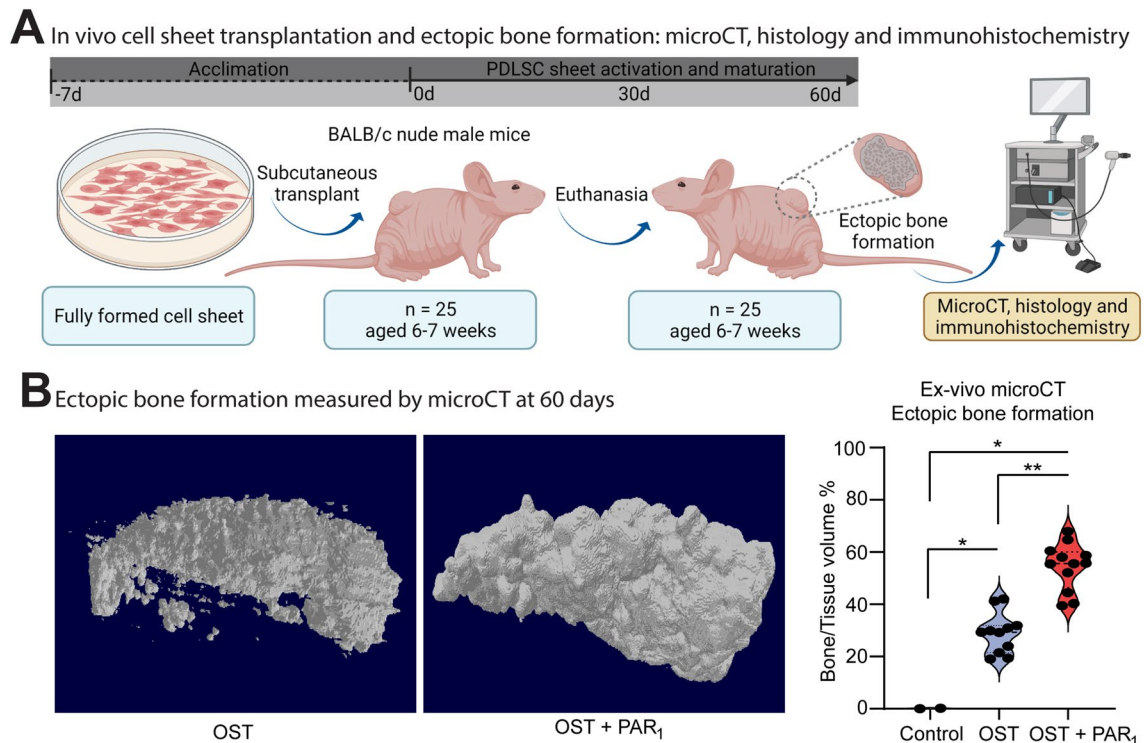


**Figure 3.** (A) Cell sheets in vivo transplant and ex-vivo analysis workflow. (B) Micro-CT analysis of ectopic bone formation in vivo after 60 days of transplantation (B) and the statistical analysis comparing the BV/TV% between the 3 groups CTRL, OST and OST + PAR<sub>1</sub>. (\*) means a  $p < 0.05$  compared to control. Results are given as the mean  $\pm$  SD. Figure (A) was created using BioRender.

Vascularization is a key mechanism in the earliest stages of osteogenesis during ectopic bone formation<sup>25,26</sup> and angiogenesis is pivotal to enabling osteogenesis in vivo<sup>27</sup>. The absence of vascularization leads to tissue necrosis through hypoxia and nutrients dearth<sup>28–30</sup>. Cell sheets present improved vessel formation capability because the space between the cell layers allows for the formation of capillaries and, therefore, vascularization in newly transplanted grafts<sup>31</sup>.

In this study, we could identify qualitative histological differences between the groups regarding angiogenesis. The CTRL group exhibited a significant number of white spots suggesting necrotic areas, possibly due to a lack of vessel formation (Fig. 4A), especially when compared with the OST and OST + PAR<sub>1</sub> groups (Fig. 4A). These findings could be explained by the absence of ascorbic acid in the CTRL group, in which depletion is related to angiogenesis impairment by inhibiting mature type IV collagen formation<sup>32</sup>. Further, the possible vascularization found in the OST group (Fig. 4A) may be explained since the group was at an earlier stage of osteogenesis when compared to the OST + PAR<sub>1</sub> group, suggesting that the osteogenesis process may have been “accelerated” by PAR<sub>1</sub> activation, which is also known to play a role in angiogenesis<sup>33–35</sup> and coagulatory pathways<sup>13</sup>. These findings corroborate with several studies that demonstrated the pro-angiogenic role of PAR<sub>1</sub> activation mainly through VEGF increased expression<sup>33–35</sup>. Further, VEGF has been shown to be an important angiogenic marker on studies evaluating the osteogenic and osteointegration processes on PDLSCs exposed to titanium-derived biomaterials *in vitro*<sup>36,37</sup>.

In fact, the enhanced osteogenic profile found in the OST + PAR<sub>1</sub> group on the histological findings was consistent with the immunohistochemistry and micro-CT results in our study (Fig. 3). Evaluation of bone volume percentage (BV/TV %) through micro-CT displayed significantly higher values in the OST + PAR<sub>1</sub> group when compared to the OST and CTRL groups (Fig. 3B).

In the bone neoformation processes, several extracellular molecules produced by differentiating osteogenic cells can be used to identify the stages of bone maturation in vivo<sup>38</sup>. Integrin 1 $\beta$  functions as a modulator, facilitating osteoblast attachment, spreading, adhesion, migration, and differentiation in osteogenesis via specific alpha(v) beta(3) signaling pathway<sup>39,40</sup> and is capable of recognizing ligands with RGD-motifs, like BSP, which works as an osteoblast differentiation marker expressed during initial stages of bone formation<sup>41,42</sup>. Further, integrin 1 $\beta$  is capable of promoting angiogenesis by mediating human endothelial cell attachment and migration<sup>40</sup> and is found to be able to integrate complexes that functions as a receptor to several collagen types<sup>43</sup>. In this matter, PAR<sub>1</sub> activation is intrinsically related to an increase in collagen deposition in fibroblasts<sup>44,45</sup> and, therefore, enhancing adhesion when integrin  $\beta$ 1 is present in the substrate<sup>46,47</sup>.

In this study, the immunohistochemistry assay results for the OST + PAR<sub>1</sub> group showed a higher protein expression for collagen type I, integrin 1 $\beta$  and BSP comparing with the other groups, evidencing an upregulated expression of important osteogenic immunological markers mediated by the PAR<sub>1</sub> activation.

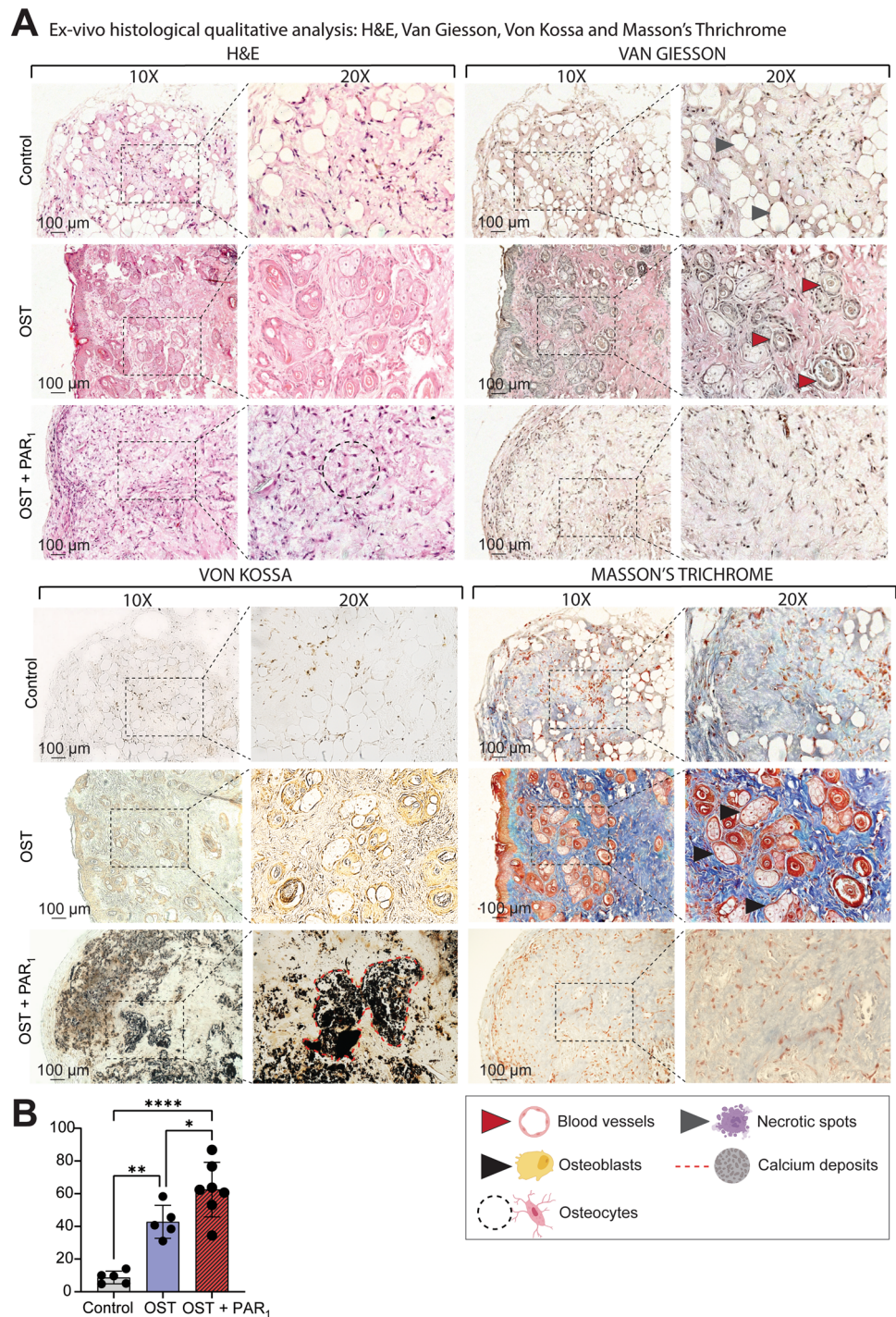
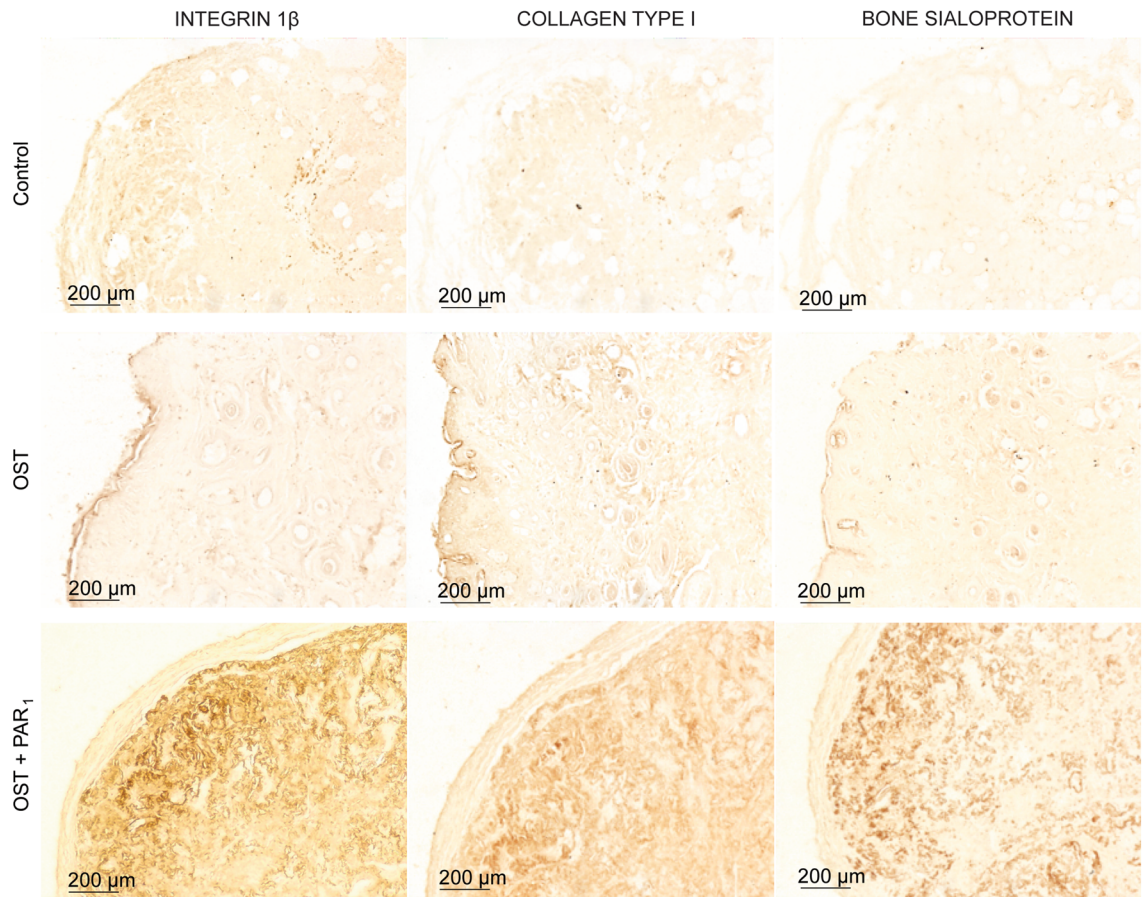


**Figure 4.** (A) Ex-vivo histological qualitative analysis from H&E, Van Gieson, Masson's Trichrome and Von Kossa stains from the 3 groups after a 2-month transplantation period in balb/c nude mice. Images at 10x and 20x. CTRL group displayed connective tissue characteristics with necrotic spots (gray arrows) and no bone formation was detected in this group for the 4 stains. Osteoblast clusters (black solid arrows) and blood vessels (red solid arrows) were detected in higher abundance in the OST group when compared with the other groups. The OST + PAR<sub>1</sub> group showed greater osteocyte numbers (black dotted circle) and higher calcium deposits (B) (red dotted line).

Finally, it is important to highlight some limitations present in this study. First, the research included only one donor cell line for the main experiments, which substantially reduces the external validity of the in vitro findings. Secondly, we found great difficulty in isolating mesenchymal strains from patients and a great difference in the

**A** Ex-vivo immunohistochemistry analysis: Integrin 1 $\beta$ , collagen type I and bone sialoprotein



**B** Immunohistochemistry quantitative analysis

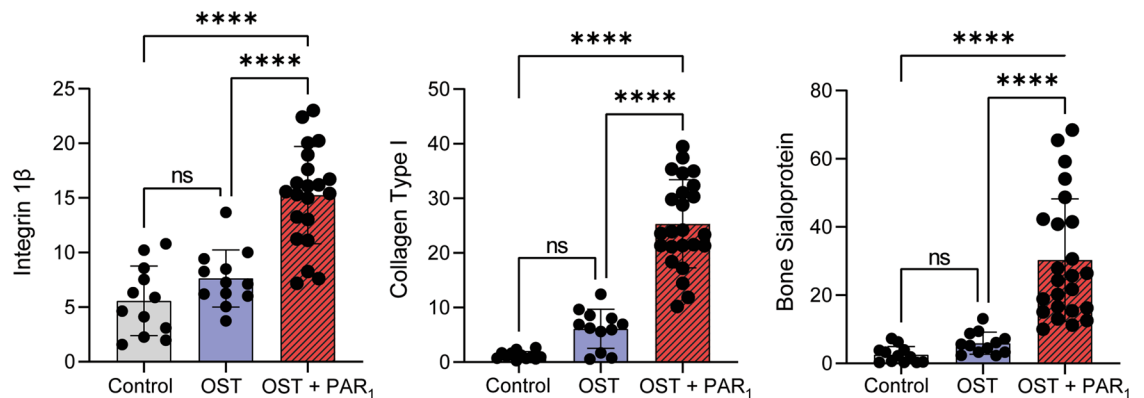


**Figure 5.** (A) Histological immunohistochemistry quantification analysis for collagen type I, integrin 1 $\beta$  and bone sialoprotein for the 3 groups *ex-vivo* samples after a 2-month transplantation period in balb/c nude mice. (B) A semi-quantification analysis was performed for the 3 protein markers and the PAR<sub>1</sub> activation group showed greater staining for the 3 osteogenic protein markers after 60 days. Images at 10x. (\*)  $p < 0.05$ . Results are given as the mean  $\pm$  SD.

surface markers characterization was found among the isolated cells. Moreover, although the flow cytometry data from the Individual 2 isolated cells were positive for a panel of surface and transcriptional factors of stemness, further differentiation into other mesenchymal cell types, i.e., adipocytes and chondrocytes, would be necessary to fully confirm their pluripotency phenotype. Yet, the osteoblastic differentiation verified in the present study suggests the therapeutic applicability in bone regeneration for PDLSCs presenting the herein characterized immunophenotyping profile. Finally, PAR<sub>1</sub> expression was found to be widely variable, limiting the receptor activation associated outcomes for further PAR<sub>1</sub> targeting therapies.

On the other hand, the use of cell sheets obtained through the removal of third molars seems to be a feasible option for further clinical therapies, since cell sheets present no associated adverse reactions because they can be obtained from and implanted in the same donor. Moreover, cell sheets are feasible to be used in regeneration procedures because the preservation of the extracellular matrix provides good structural stability and manageability, allowing this tissue engineering strategy to have a promising future as an option in regenerative treatments.

The main finding of this study is that the PAR<sub>1</sub> activation in PDLSCs cell sheets enhanced osteogenesis *in vivo*. In addition, *in vitro* results from ARS reinforced that the presence of cell phenotype for stemness and PAR<sub>1</sub> surface biomarkers are associated with an upregulation of osteogenesis in PDLSCs.

## Methods

We confirm that all methods were carried out in accordance with ARRIVE guidelines and relevant guidelines and regulations.

**Ethics Statement.** Informed consent was obtained from all subjects and the ethical committee approval from the Ethics Committee Review Board at the School of Dentistry of the University of São Paulo (FO-USP-protocol number 029/2018) was obtained prior to the patient's teeth collection at the clinic of the School of Dentistry of the University of São Paulo (FO-USP). The utilization of Balb/c nude mice in this research was also approved by the Ethics Committee on Animal Use (CEUA) board at the Chemistry Institute of the University of São Paulo (IQ-USP) under the protocol number 98/2018.

**Cells isolation.** Periodontal ligament stem cells were harvested from third molars from 3 systemically healthy individuals (I1, I2 and I3—18 to 30 years old). The inclusion criteria were: partially or totally erupted third molars and absence of periodontal disease.

Periodontal ligament tissue specimens were obtained through the scaling of the middle third of the root and PDLSCs were isolated using the explant technique<sup>12,48</sup> in alpha-modified Eagle's medium ( $\alpha$ -MEM) (Thermo Fisher Scientific, Waltham, USA) supplemented with 10% fetal bovine serum (FBS) (Thermo Fisher Scientific, Waltham, USA), 100  $\mu$ g/mL penicillin, 100  $\mu$ g/mL streptomycin, and 0.5 mg/mL amphotericin B (Gibco, Invitrogen, Carlsbad, USA) at 37 °C in an atmosphere of 5% CO<sub>2</sub> and 95% humidity<sup>7</sup>. After 14 days, cells from the explants achieved a 70% confluence degree and PDLSCs populations were used in passage 4 for all experiments.

**Pluripotency characterization.** In order to identify the mesenchymal stem cell phenotype, approximately  $5 \times 10^5$  PDLSCs were incubated in 5% bovine serum albumin (BSA)/phosphate buffered saline (PBS) (Gibco, Invitrogen, Carlsbad, USA)  $1 \times$  at 4 °C in dark for 1 h with the following monoclonal antibodies: PAR<sub>1</sub>-FITC (Abcam, Cambridge, UK), OCT4-FITC (Abcam, Cambridge, UK), SOX2-FITC (Abcam, Cambridge, UK), STRO-1-FITC (Abcam, Cambridge, UK), CD14-FITC (eBioscience, San Diego, USA), CD90-FITC (eBioscience, San Diego, USA), CD31-PE (eBioscience, San Diego, USA), CD-44-PE (eBioscience, San Diego, USA), CD34-FITC (Biolegend, San Diego, USA) and CD146-PE (Biolegend, San Diego, USA) for 30 min at 4 °C. Unstained control was used to set gates. A total of 10–50,000 events were recorded and data analyzed through FlowJo (Becton Dickinson, Oregon, USA).

**Cell sheet culture and experimental design.** PDLSCs at  $1 \times 10^6$  cells/cm<sup>2</sup> were seeded in 100 mm plates for 24 h with  $\alpha$ -MEM (Thermo Fisher Scientific, Waltham, USA) supplemented with 10% of FBS (Thermo Fisher Scientific, Waltham, USA) and 50  $\mu$ g/mL vitamin C to induce cell sheet formation, as previously described<sup>7</sup>. Subsequently, cell sheets were assigned for one of the following experimental groups: (1) control medium (CTRL) composed of  $\alpha$ -MEM (Thermo Fisher Scientific, Waltham, USA) supplemented with 10% of FBS (Thermo Fisher Scientific, Waltham, USA) and 50  $\mu$ g/mL vitamin C (Sigma-Aldrich, St Louis, USA); (2) osteogenic medium (OST) (CTRL + 100 nM dexamethasone, 5 mM  $\beta$ -glycerophosphate and 50  $\mu$ g/ml ascorbic acid (Sigma-Aldrich, St Louis, USA) and (3) osteogenic medium with the addition the PAR<sub>1</sub> agonist peptide (100 nM TFLLR-NH<sub>2</sub>) (Tocris Bioscience Inc., Bristol, UK) (OST + PAR<sub>1</sub>). The culture medium was changed every 3 days for 14 days.

**Alizarin red staining.** The PDLSCs from I2 were seeded in 6-well plates ( $5 \times 10^4$  cells/cm<sup>2</sup>), in triplicate. After treatment with CTRL, OST and OST + PAR<sub>1</sub> groups for 14 days, cell sheets were washed with  $1 \times$  PBS (Sigma-Aldrich, St Louis, USA), fixed with 4% paraformaldehyde (Sigma-Aldrich, St Louis, USA) for 15 min at room temperature (RT), washed with  $1 \times$  PBS (Sigma-Aldrich, St Louis, USA) again and incubated with a stirring solution of 2% Alizarin Red S (Sigma-Aldrich, St Louis, USA) in PBS (Sigma-Aldrich, St Louis, USA) (pH 4.2) (A5533) for 30 min at RT. For qualitative and macroscopic analysis, images were acquired using a microscope CDD camera (D7000, Nikon, Minato, Japan). For the quantitative analysis, 10% ammonium hydroxide (Sigma-Aldrich, St Louis, USA) solution was used to dilute calcium deposits and a spectrophotometer (Biotek, Winooski, USA) was used to measure the absorbance at 405 nm. ARS quantification was calculated using a standard-curve.

**Cell sheet characterization.** *Scanning electron microscopy.* Cell sheets at 14-days treatment were fixed with Karnovsky's solution (Thermo Fisher Scientific, Waltham, USA) for 24 h. After this period, post-fixation was performed with osmium tetroxide (Sigma-Aldrich, St Louis, USA) for 2 h and dehydration, passing the material through an increasing series of alcohol (Sigma-Aldrich, St Louis, USA) from 70 to 100%. The samples were further dried under critical point conditions and sputter coated with gold. Observations were then performed by using a scanning electron microscope (S-4800; Hitachi, Tokyo, Japan).



**Histological profile.** Hematoxylin and eosin (Sigma-Aldrich, St Louis, USA) staining of cell sheets was also performed. Briefly, after detachment and fixation in 4% paraformaldehyde (Sigma-Aldrich, St Louis, USA) for 24 h, samples were paraffin embedded and sectioned in 4  $\mu\text{m}$  thickness. After the sectioning process, the histological samples were placed in a water bath at 50 °C and captured to a histological slide and stored in an oven at 65 °C for 12 h to allow the paraffin remnants to be removed. Sequentially, paraffin removal dehydration protocol was completed using a sequence of xylol (Sigma-Aldrich, St Louis, USA) and alcohol (Sigma-Aldrich, St Louis, USA) solutions and the specimens proceeded a routine H&E staining following the manufacturer's guidelines.

**Ectopic bone formation assays.** In vivo bone formation was evaluated using transplantation of cell sheets pre-incubated with the experimental groups described above. At 14 days of incubation, cell sheets were detached using a cell scraper (Corning, New York, USA), folded 4 times to acquire a cylinder shape and each 6-weeks old Balb/c nude mice received 2 dorsal transplants from the same experimental group, bilaterally. In total, 25 mice were distributed to the groups as follows: 11 (OST + PAR<sub>1</sub>), 11 (OST) and 3 (CTRL). After 60 days, mice were euthanized and the subcutaneous samples were removed and processed for the analysis described below.

**Computerized microtomography.** After fixation, only the left side subcutaneous sample from each animal was scanned using a micro-CT system (Skyscan 1176, Bruker Biospin, Billerica, USA) with the following acquisition parameters: 45 kV, 8.71  $\mu\text{m}$  resolution and 550  $\mu\text{A}$ . Data obtained were processed, reconstructed into three-dimensional images using a reconstruction software (NRecon, Micro Photonics, Allentown, USA) and analyzed using a system software (CTAn, Bruker Biospin, Billerica, USA).

**Immunohistochemistry and histological analysis.** Histological procedures were performed as described previously. H&E, Masson's Trichrome, Van Gieson and Von Kossa stains (Sigma-Aldrich, St Louis, USA) were carried out following the manufacturer's protocol. For immunohistochemistry analysis, after fixation in a 4% paraformaldehyde solution in PBS for 30 min, the samples were embedded in paraffin and sectioned at 20  $\mu\text{m}$ . Cuts were subjected to dewaxing, rehydration, and permeabilized with 0.2% Triton X-100 (Sigma-Aldrich, St Louis, USA) for 10 min. Then, the sections were blocked in 3% hydrogen peroxide solution (Sigma-Aldrich, St Louis, USA) for 10 min followed by antigen retrieval with 10% citrate buffer (Sigma-Aldrich, St Louis, USA) for 15 min and blockage in 5% BSA (Sigma-Aldrich, St Louis, USA) for another 30 min. Then, exposure to the specific primary antibodies was performed for:  $\beta$ 1 integrin—AB52971 (Abcam, Cambridge, UK), type I collagen—AB34710 (Abcam, Cambridge, UK), and BSP—AB8448 (Abcam, Cambridge, UK). The slides were then incubated with a secondary conjugated anti-rabbit IgG antibody—AB205718 (Abcam, Cambridge, UK) followed by an avidin-biotin complex (Abcam, Cambridge, UK) incubation for 30 min. The diaminobenzidine (DAB) solution (Abcam, Cambridge, UK) was applied every 2 min and the reaction was observed in a microscope. Specimens were dehydrated, cleared and mounted. Images from the specimens were obtained with a light microscope (E600, Nikon, Tokyo, Japan) and three images of each sample were acquired and quantified using Image J (NIH, Bethesda, USA).

**Statistical analysis.** Experiments were performed in triplicate and data were expressed as means  $\pm$  standard deviation (SD). Data were analyzed based on the comparison between the experimental group (OST + PAR<sub>1</sub>) with the osteogenic control group (OST) and the control (CTRL). One-way ANOVA followed with post-hoc Tukey's test was used. A significance *P* value of 0.05 was established for all tests and the data analysis was performed (GraphPad Prism™ Version 6.0c, La Jolla, USA).

## Data availability

The datasets used and/or analysed during the current study available from the corresponding author on reasonable request.

Received: 24 June 2022; Accepted: 30 August 2022

Published online: 18 September 2022

## References

- Caton, G. *et al.* A new classification scheme for periodontal and peri-implant diseases and conditions—Introduction and key changes from the 1999 classification. *J. Clin. Periodontol.* **45**, S1–S8 (2018).
- Magnusson, I., Runstad, L., Nyman, S. & Lindhe, J. A long junctional epithelium—A locus minoris resistentiae in plaque infection?. *J. Clin. Periodontol.* **10**, 333–340 (1983).
- Gao, L. N. *et al.* The effect of the coumarin-like derivative osthole on the osteogenic properties of human periodontal ligament and jaw bone marrow mesenchymal stem cell sheets. *Biomaterials* **34**, 9937–9951 (2013).
- Kim, K., Utoh, R., Ohashi, K., Kikuchi, T. & Okano, T. Fabrication of functional 3D hepatic tissues with polarized hepatocytes by stacking endothelial cell sheets in vitro. *J. Tissue Eng. Regen. Med.* **11**, 2071–2080 (2017).
- Mackie, E. J. *et al.* Protease-activated receptors in the musculoskeletal system. *Int. J. Biochem. Cell Biol.* **40**, 1169–1184 (2008).
- Ramachandran, R., Altier, C., Oikonomopoulou, K. & Hollenberg, M. D. Proteinases, their extracellular targets, and inflammatory signaling. *Pharmacol. Rev.* **68**, 1110–1142 (2016).
- Mendoza, A. H., Balzarini, D., Alves, T., Rovai E. S. & Holzhausen, M. Potential of mesenchymal stem cell sheets on periodontal regeneration: A systematic review of pre-clinical studies. *Syst. Rev. Article*. <https://doi.org/10.2174/1574888x17666220706092520> (2022).
- Kim, J.-H. *et al.* Tumor necrosis factor- $\alpha$  antagonist diminishes osteocytic RANKL and sclerostin expression in diabetes rats with periodontitis. *PLoS ONE* **12**, e0189702 (2017).
- Rovai, E. S. *et al.* Protease-activated receptor type 1 (PAR1) increases CEMP1 gene expression through MAPK/ERK pathway. *Braz. Oral Res.* **36**, 1–8 (2022).

10. Sato, N. *et al.* Thrombin induced by the extrinsic pathway and PAR1 regulated inflammation at the site of fracture repair. *Bone* **83**, 23–34 (2016).
11. Abraham, L. A. & Mackie, E. J. Modulation of osteoblast-like cell behavior by activation of protease-activated receptor-1. *J. Bone Miner. Res.* **14**, 1320–1329 (1999).
12. Arayatrakoollikit, U., Pavasant, P. & Yongchaitrakul, T. Thrombin induces osteoprotegerin synthesis via phosphatidylinositol 3'-kinase/mammalian target of rapamycin pathway in human periodontal ligament cells. *J. Periodontol. Res.* **43**, 537–543 (2008).
13. Rovai, E. S., Alves, T. & Holzhausen, M. Protease-activated receptor 1 as a potential therapeutic target for COVID-19. *Exp. Biol. Med.* **246**, 688–694 (2021).
14. Song, S. J., Pagel, C. N., Campbell, T. M., Pike, R. N. & Mackie, E. J. The role of protease-activated receptor-1 in bone healing. *Am. J. Pathol.* **166**, 857–868 (2005).
15. Choi, J. K., Hwang, H. I. & Jang, Y. J. The efficiency of the in vitro osteo/dentinogenic differentiation of human dental pulp cells, periodontal ligament cells and gingival fibroblasts. *Int. J. Mol. Med.* **35**, 161–168 (2015).
16. Jastrzebski, S. *et al.* Protease-activated receptor 1 deletion Causes enhanced osteoclastogenesis in response to inflammatory signals through a notch2-dependent mechanism. *J. Immunol.* **203**, 105–116 (2019).
17. Rovai, E. S. *et al.* Protease-activated receptor type 1 activation enhances osteogenic activity in human periodontal ligament stem cells. *Stem Cells Int.* **2019**, 6857386 (2019).
18. Xu, J., Wang, W., Kapila, Y., Lotz, J. & Kapila, S. Multiple differentiation capacity of STRO-1 +/CD146 + PDL mesenchymal progenitor cells. *Stem Cells Dev.* **18**, 487–496 (2009).
19. Fujii, S. *et al.* Investigating a clonal human periodontal ligament progenitor/stem cell line in vitro and in vivo. *J. Cell. Physiol.* **215**, 743–749 (2008).
20. Gay, I. C., Chen, S. & MacDougall, M. Isolation and characterization of multipotent human periodontal ligament stem cells. *Orthod. Craniofacial Res.* **10**, 149–160 (2007).
21. Nagatomo, K. *et al.* Stem cell properties of human periodontal ligament cells. *J. Periodontol. Res.* **41**, 303–310 (2006).
22. Chen, S. C., Marino, V., Gronthos, S. & Bartold, P. M. Location of putative stem cells in human periodontal ligament. *J. Periodontol. Res.* **41**, 547–553 (2006).
23. Kémoun, P. *et al.* Localization of STRO-1, BMP-2/-3/-7, BMP receptors and phosphorylated Smad-1 during the formation of mouse periodontium. *Tissue Cell* **39**, 257–266 (2007).
24. Kémoun, P. *et al.* Human dental follicle cells acquire cementoblast features under stimulation by BMP-2/-7 and enamel matrix derivatives (EMD) in vitro. *Cell Tissue Res.* **329**, 283–294 (2007).
25. Gerber, H. P. & Ferrara, N. Angiogenesis and bone growth. *Trends Cardiovasc. Med.* **10**, 223–228 (2000).
26. Bragdon, B. *et al.* Earliest phases of chondrogenesis are dependent upon angiogenesis during ectopic bone formation in mice. *Bone* **101**, 49–61 (2017).
27. Amini, A. R., Laurencin, C. T. & Nukavarapu, S. P. Bone tissue engineering: Recent advances and challenges. *Crit. Rev. Biomed. Eng.* **40**, 363–408 (2012).
28. Novosel, E. C., Kleinhans, C. & Kluger, P. J. Vascularization is the key challenge in tissue engineering. *Adv. Drug Deliv. Rev.* **63**, 300–311 (2011).
29. Phelps, E. A. & García, A. J. Engineering more than a cell: Vascularization strategies in tissue engineering. *Curr. Opin. Biotechnol.* **21**, 704–709 (2010).
30. Li, R. *et al.* Preparation of three-dimensional vascularized msc cell sheet constructs for tissue regeneration. *Biomed Res. Int.* **2014**, (2014).
31. Sakaguchi, K., Shimizu, T. & Okano, T. Construction of three-dimensional vascularized cardiac tissue with cell sheet engineering. *J. Control. Release* **205**, 83–88 (2015).
32. Telang, S., Clem, A. L., Eaton, J. W. & Chesney, J. Depletion of ascorbic acid restricts angiogenesis and retards tumor growth in a mouse model. *Neoplasia* **9**, 47–56 (2007).
33. Ma, L. *et al.* Proteinase-activated receptors 1 and 4 counter-regulate endostatin and VEGF release from human platelets. *Proc. Natl. Acad. Sci. USA* **102**, 216–220 (2005).
34. Yin, Y. *et al.* Oncogenic transformation induces tumor angiogenesis: A role for PAR1 activation. *FASEB J.* **17**, 163–174 (2003).
35. Hu, S., Wu, G., Zheng, J., Liu, X. & Zhang, Y. Astrocytic thrombin-evoked VEGF release is dependent on p44/42 MAPKs and PAR1. *Biochem. Biophys. Res. Commun.* **509**, 585–589 (2019).
36. Diomede, F. *et al.* VEGF/VEGF-R/RUNX2 Upregulation in human periodontal ligament stem cells seeded on dual acid etched titanium disk. *Materials (Basel)*. **13**(3), 706 (2020).
37. Marconi, G. D. *et al.* Enhanced VEGF/VEGF-R and RUNX2 Expression in human periodontal ligament stem cells cultured on sandblasted/etched titanium disk. *Front. Cell Dev. Biol.* **8**, 315 (2020).
38. Lekic, P., Sodek, J. & McCulloch, C. A. G. Osteopontin and bone sialoprotein expression in regenerating rat periodontal ligament and alveolar bone. *Anat. Rec.* **244**, 50–58 (1996).
39. Campbell, I. D. & Humphries, M. J. Integrin structure, activation, and interactions. *Cold Spring Harb. Perspect. Biol.* **3**, 1–14 (2011).
40. Bellahcène, A. *et al.* Bone sialoprotein mediates human endothelial cell attachment and migration and promotes angiogenesis. *Circ. Res.* **86**, 885–891 (2000).
41. Marom, R., Shur, I., Solomon, R. & Benayahu, D. Characterization of adhesion and differentiation markers of osteogenic marrow stromal cells. *J. Cell. Physiol.* **202**, 41–48 (2005).
42. Harris, N. L. *et al.* Functional analysis of bone sialoprotein: Identification of the hydroxyapatite-nucleating and cell-binding domains by recombinant peptide expression and site-directed mutagenesis. *Bone* **27**, 795–802 (2000).
43. Leitinger, B. & Hohenester, E. Mammalian collagen receptors. *Matrix Biol.* **26**, 146–155 (2007).
44. Fiorucci, S. *et al.* PAR1 Antagonism protects against experimental liver fibrosis. Role of proteinase receptors in stellate cell activation. *Hepatology* **39**, 365–375 (2004).
45. Shi, G. *et al.* Apixaban attenuates ischemia-induced myocardial fibrosis by inhibition of Gq/PKC signaling. *Biochem. Biophys. Res. Commun.* **500**, 550–556 (2018).
46. Kanemaru, M., Maehara, N., Iwamura, T. & Chijiwa, K. Thrombin stimulates integrin  $\beta$ 1-dependent adhesion of human pancreatic cancer cells to vitronectin through protease-activated receptor (PAR)-1. *Hepatogastroenterology.* **59**, 1614–1620 (2012).
47. Rudroff, C., Striegler, S., Schilli, M. & Scheele, J. Thrombin enhances adhesion in pancreatic cancer in vitro through the activation of the thrombin receptor PAR 1. *Eur. J. Surg. Oncol.* **27**, 472–476 (2001).
48. Somerman, M. J., Archer, S. Y., Imm, G. R. & Foster, R. A. A comparative study of human periodontal ligament cells and gingival fibroblasts in vitro. *J. Dent. Res.* **67**, 66–70 (1988).

## Acknowledgements

This work was supported by the São Paulo Research Foundation (FAPESP) grants 2017/23158-0 and 2018/13818-5, the Coordination for the Improvement of Higher Education Personnel—(CAPES) Finance code 001 and the J. William Fulbright scholarship. Figures were produced using BioRender.

### Author contributions

T.A., L.M.G., E.A. and M.H. conceived and designed the experiments; T.A., L.M.G., D.B., V.O., J.S., and A.H. performed the experimental work and contributed to the manipulation of materials, reagents, and analysis tools; T.A., D.B., and J.S. performed animal experiments; T.A. and E.A., analyzed the data and wrote the manuscript. T.A. drafted the major portion of the manuscript and M.H., E.A., E.S.R., L.H.C. and C.R.S. contributed with major revisions. T.A., M.H., E.S.R. and A.H. contributed with the final revisions. T.A. and L.M.G. structured the figures. All authors read and approved the final manuscript.

### Competing interests

The authors declare no competing interests.

### Additional information

**Supplementary Information** The online version contains supplementary material available at <https://doi.org/10.1038/s41598-022-19520-x>.

**Correspondence** and requests for materials should be addressed to M.H.

**Reprints and permissions information** is available at [www.nature.com/reprints](http://www.nature.com/reprints).

**Publisher's note** Springer Nature remains neutral with regard to jurisdictional claims in published maps and institutional affiliations.



**Open Access** This article is licensed under a Creative Commons Attribution 4.0 International License, which permits use, sharing, adaptation, distribution and reproduction in any medium or format, as long as you give appropriate credit to the original author(s) and the source, provide a link to the Creative Commons licence, and indicate if changes were made. The images or other third party material in this article are included in the article's Creative Commons licence, unless indicated otherwise in a credit line to the material. If material is not included in the article's Creative Commons licence and your intended use is not permitted by statutory regulation or exceeds the permitted use, you will need to obtain permission directly from the copyright holder. To view a copy of this licence, visit <http://creativecommons.org/licenses/by/4.0/>.

© The Author(s) 2022